CARDIOPULMONARY AUSCULTATION SYSTEM ENABLED BY A NOVEL BEYOND-RESONANCE SENSING ACCELEROMETER

Tzeno Galchev[1], Longwei Xiao[2], Wenyong Zhang[2], Haozhe Dong[2], Jianglong Zhang[1], James Lin[1], Zhengxin Zhao[1], Adam Spirer[1], Jin Peng[3], Hua Jiang[4], Khiem Nguyen[1], and Sam Zhang[1]
[1]Analog Devices, Inc., Massachusetts, USA
[2]Catron Inc., Minnesota, USA
[3]Department of Neuroscience, Histology, and Embryology, Sichuan University, China
[4]Sichuan Provincial People's Hospital, China

ABSTRACT

This paper presents a new chest patch for cardiopulmonary auscultation and vital-sign monitoring. The system houses a tri-axial accelerometer, a photoplethysmography (PPG) module, and an electrocardiography (ECG) module for the simultaneous and synchronized collection of seismocardiography (SCG), PPG (heart rate (HR), oxygen saturation (SpO2), respiratory rate (RR) interval), ECG, and lung auscultation. The SCG and lung auscultation depend on a new 16-bit, digital, ultra-low-noise, low-power, and high-bandwidth MEMS accelerometer that utilizes a novel sensing technique called beyond-resonance sensing (BRS) to achieve a 4 kHz bandwidth with very low noise density (<29 µg/√Hz) in a compact 2.9×2.8×0.87 mm^3 form-factor. The system is prototyped, and data is collected on a human subject demonstrating both heart and lung auscultation.

KEYWORDS

Seismocardiography; Lung-auscultation; Vital-sign monitoring; Beyond-resonance sensing accelerometer

INTRODUCTION

In the United States a person dies from cardiovascular disease (CVD) approximately every 45 seconds [1]. It is the leading cause of death globally according to the World Health Organization (WHO) with 17.9 million deaths per year [2]. One third of those deaths occur prematurely before the age of 70. Similarly, chronic obstructive pulmonary disease (COPD) is the third leading cause of death worldwide. The two terms CVD and COPD are both umbrella names that have to do with diseases of the heart and lungs that develop slowly over time, impact blood and airflow, cause discomfort, difficulty breathing, impact mobility, and are degenerative. Furthermore, heart failure (HF) and COPD both have characteristic exacerbations which ultimately lead to hospitalizations if not managed effectively. It is estimated that global economic burden for CVD and COPD is expected to grow to $4.8T dollars worldwide [3]. With such a high cost and incidence level, the case for early detection and new disease management modalities is clear. Detecting the early signs of either disease is tricky since symptoms may be minute and not easily identifiable during annual check-ups. Furthermore, disease management is problematic because by the time symptoms have worsened to the point that people are seeking medical attention, multiple easier, less expensive, and less invasive treatment options may no longer be possible.

Wearable electronics have a role to play in helping with disease diagnostics, monitoring, and management. Modern wearables for fitness and lifestyle, whether they be various smart watches or fitness chest straps, already contain sensors with the capability of multi-thousand-dollar hospital bench equipment. Therefore, the capability to collect, transmit, and interpret large amounts of vital-sign information and insights exists and is readily expanding. However, to diagnose a wider range of cardiac and respiratory

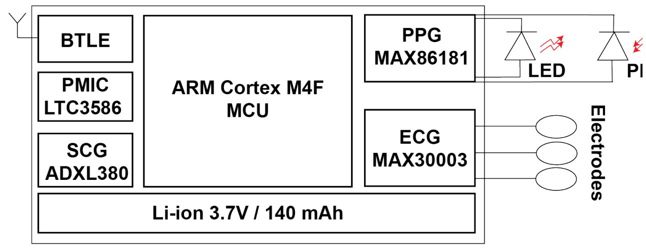

Figure. 1. Block diagram of the vital-sign monitoring patch.

conditions, more capability is required. For example, while photoplethysmography (PPG) and electrocardiography (ECG) have become commonplace in consumer wearables, both methods produce information with insufficient resolution to the underlying physiological processes. While ECG is one of the most commonplace tests done in a hospital, it provides superficial information on the various cardiac processes taking place because it is a measure of the total electrical activity of the heart muscle. Similarly, PPG is a measurement of the volumetric change of blood and therefore able to capture cardiac activity at a high level. On the other hand, seismocardiography (SCG) [4] is a measurement of the vibrations in the chest cavity, produced by the beating of the heart. Each beat of the heart is characterized by several events such as opening and closing of valves, blood flowing in and out of the heart, contractions of the atriums and ventricles, all of which produce mechanical signatures and vibrations that can be sensed and analyzed. Another common exam administered during a hospital visit is pulmonary auscultation by physicians using a stethoscope. The sounds generated by airflow in and around the lungs carries important information. Abnormalities such as crackles, wheezing, rhonchi, and others can indicate a variety of pulmonary illnesses [5]. Changes in wheezing, for example, can indicate early signs of COPD or asthma. Additionally, respiratory rate (RR) is a key monitor to track the progression of illness [6].

Prior efforts that aim to pick up not just RR but also lung sounds have mostly relied on microphones for the auscultation [7, 8], whereas here we have utilized an accelerometer. Microphones are sensitive to ambient noise and require significant and power-hungry post processing. Compact, low-cost, and low-power commercial accelerometers to date lack the signal-to-noise (SNR) performance and bandwidth for lung-auscultation. Abnormal lung sounds contain spectral content between 100-5000 Hz [5]. That is why previous efforts that use inertial sensing have relied on highly custom devices [9]. Similarly, SNR is important to SCG collection where typical vibrations would reside in the 10 mgee range (1 gee = 9.8 m/s^2) [10], with a bandwidth of interest in the 1-100 Hz range.

This paper presents a new wireless chest patch for cardiopulmonary auscultation and vital-sign monitoring (VSM). The key technological novelty hinges on a new, tri-axial, ultra-low-noise, low-power, and high-bandwidth accelerometer that enables high-fidelity SCG and lung sound detection. The chest patch further

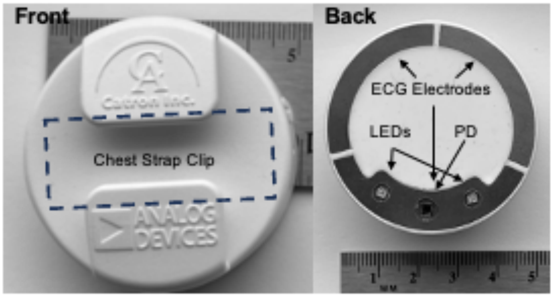

Figure 2. Photograph of the fully assembled VSM patch.

integrates PPG and ECG. This makes it possible to simultaneously collect SCG, HR, blood oxygen saturation (SpO2), RR, and lung auscultation. With all these key vital-sign markers it is feasible to infer a great deal about the current health of the person, trends over time, and one could theorize that with more investigation this information can lead to accurate predictions of the future state of health.

SYSTEM DESIGN

The VSM system discussed in this work is designed to be placed on the chest and has a nook through which one can run an elastic chest strap to secure the system in place. A functional block diagram is shown in Figure 1. The system uses three separate sensors from Analog Devices including the ADXL380 tri-axial accelerometer, the MAX86181 integrated optical module, and the MAX300003 single channel biopotential analog front end. Data is captured simultaneously, buffered, and transferred to a PC application via Bluetooth for further processing, storage and display. The system has a diameter of 50 mm and thickness of 23 mm. A photograph of the assembled chest patch is shown in Figure 2. The stainless-steel ECG electrodes can be seen on the back along with the pockets for the LEDs and photodiode.

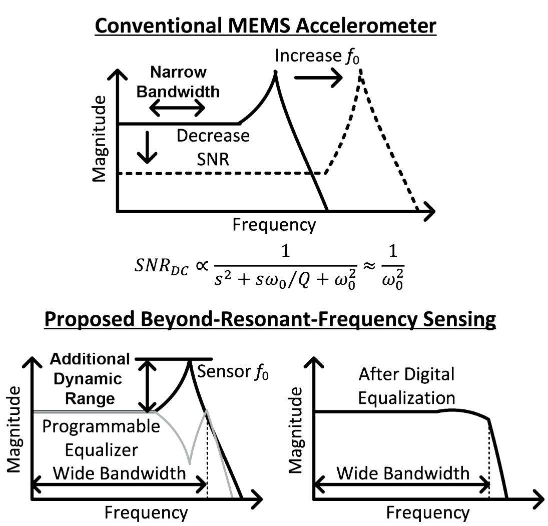

Figure 3. Beyond-resonance-sensing (BRS) accelerometer concept.

WIDE-BANDWIDTH ACCELEROMETER

The chest patch uses a new accelerometer made possible by a novel beyond resonance sensing (BRS) technique. A typical accelerometer faces a tradeoff between SNR (noise performance), and bandwidth as shown in Figure 3. To reduce the noise, one can either add more mass, *m*, or increase the quality factor, *Q*, however both will lower the effective bandwidth of the accelerometer. The

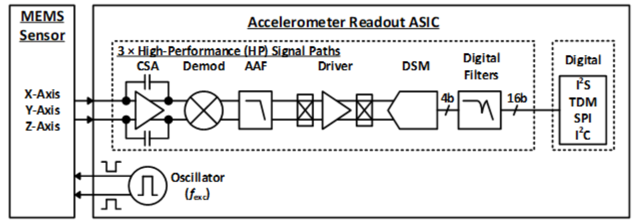

Figure 4. Block diagram of the 16-bit tri-axial MEMS accelerometer readout ASIC.

bandwidth is defined as the flat part of the transfer function over frequency. Similarly, to increase the bandwidth, one must make the accelerometer stiffer (higher spring constant) or reduce the mass both of which will tend to increase the noise. The BRS concept is described in the bottom part of Figure 3. To get around the tradeoff between SNR and bandwidth, the idea is to use the entire response of the mechanical sensor, including the area around its fundamental frequency (f_o) and inherent resonance response governed by the quality factor (Q) of the sensor [11]. The response is sensed, digitized, and then “corrected” to remove the resonance effect, and flatten the sensitivity over frequency using a digital equalization (EQ) technique. One of the main challenges with this approach is that now the ASIC must have a dynamic range that is Q-times higher than the required full-scale range of the accelerometer.

Figure 4 shows the block diagram of the MEMS accelerometer readout ASIC. The readout ASIC performs two key functions: drives the sensor with a set of excitation signals and senses the capacitance change of the sensor. On the drive side, an oscillator provides a set of clock signals to the sensor modulating the acceleration signals to the excitation frequency (f_{exc}) of around 64 kHz. On the sense side, three 16-bit high-performance signal paths demodulate and measure the capacitance change of the tri-axial MEMS sensor beyond the resonance of the sensor. To sense acceleration robustly in the presence of mechanical gain, the analog front-end is designed to have a wide-bandwidth (BW) and a large dynamic range (DR) to digitize the entire mechanical response. Each channel consists of a charge-sensitive amplifier (CSA), a demodulator (demod), an anti-aliasing filter (AAF), an ADC driver, a discrete-time second-order delta-sigma modulator (DSM), and digital filters.

The CSA is configured as an amplifier with capacitive feedback to sense the modulated acceleration signal around 64 kHz. The CSA’s outputs are demodulated by f_{exc} down to baseband. Once demodulated, the signals are filtered by an AAF to remove high-frequency noise. Following that, an ADC driver delivers the signals to a discrete-time second-order DSM for digitization. The choice of a second-order DSM architecture is due to its noise-shaping characteristics and its capability to handle a large input range. This is particularly desirable as the BRS technique requires additional DR to accommodate the mechanical gain at the sensor’s resonance. For power consumption and DR considerations, the DSM has a sampling frequency of 512 kHz, an oversampling ratio (OSR) of 64, and a 4-bit SAR ADC as its quantizer. This yields a measured DR of 93.3 dBFS with a BW of 4 kHz while consuming 38 µA from a 1.8 V supply resulting in an ADC figure-of-merit (FoM) [12] of 171.0 dB. Once the signals are converted to the 4-bit bit-streams, they are decimated, equalized, and low-pass filtered to the final output data rate (ODR) of 8 kS/s by the digital filters. The digital equalization (EQ) coefficients are programmed based on measured sensor response at test to restore the flatness of the signal transfer function of each part. The digitized acceleration signals are communicated off-chip through one of the many supported protocols at 8 kS/s with a sensing BW of 4 kHz.

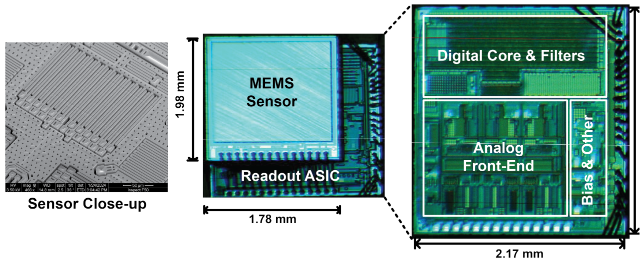

Figure 5. Fabricated BRS accelerometer with ASIC close-up and partial SEM of the sensor die.

The capacitive accelerometer is made using Analog Devices' commercial surface-micromachining process. It has a 16 µm thick polysilicon beam for the active element of the mechanical sensor and is capped in moderate vacuum. The accelerometer die is 1.78×1.98 mm^2. The ASIC is fabricated using a commercial 0.18-µm CMOS process and measures 2.17×2.32 mm^2. The ASIC and MEMS sensor are stacked and packaged together in a land grid array (LGA) package measuring 2.9×2.8×0.87 mm^3. Figure 5 shows close-ups of the fabricated ASIC and MEMS sensors as well as the stack-up.

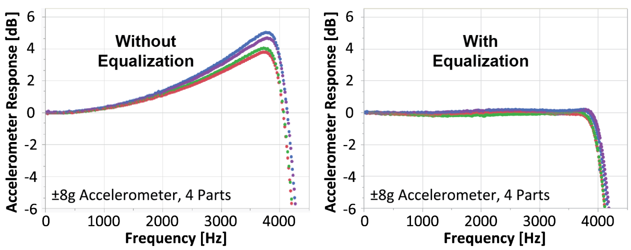

Figure 6. Frequency response of BRS accelerometer with and w/o equalization.

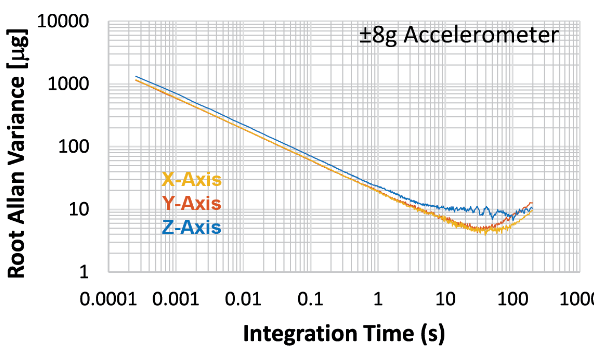

Figure 7. Allan variance of all three BRS accelerometer axes in ±8 gee full-scale range.

The packaged sensor is placed on a piezoelectric shaker, configured to operate in ±8g full-scale range and actuated using a sine sweep from 10 Hz – 10 kHz at 2 gee, while the response is monitored using a reference accelerometer. The accelerometer has an f_o of 4.06 kHz (xy-axis) and 3.5 kHz (z-axis). Figure 6 shows the frequency response of the accelerometer with and without the EQ turned on. While enabled, the EQ delivers a bandwidth flatness of of ±0.56 dB up to 3.8 kHz. The -3 dB bandwidth of the accelerometer is 4 kHz. The Allan variance of the three accelerometer axes is shown in Figure 7 while operating in ±8 gee full-scale range. The measured noise density for x- and y-axis is 22 µg/√Hz and z-axis is 29 µg/√Hz. The BRS accelerometer consumes 374 µA using a 1.8V supply at room temperature. The combination

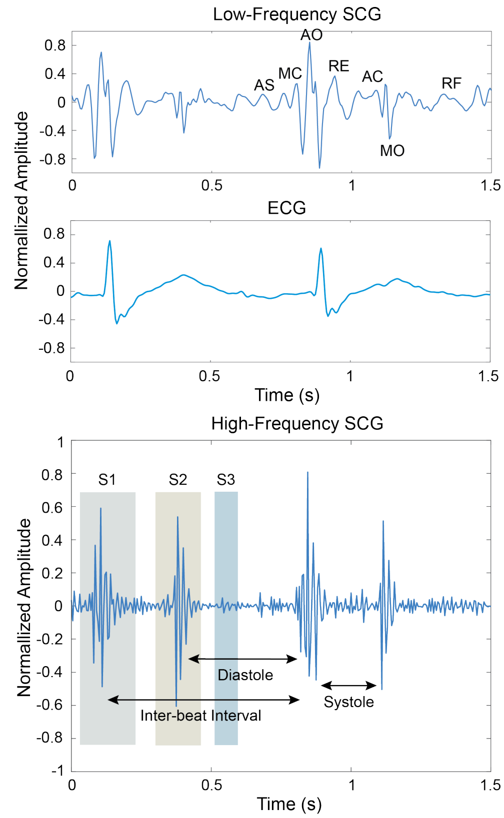

Figure 8. The top plot shows the measured and time-synchronized ECG and low-frequency (raw) SCG signal with markers for the relevant cardiac cycle events. Bottom plot shows the high-pass filtered response revealing the S_1, S_2 and S_3 heart-sounds.

of SNR, usable bandwidth, and low current consumption demonstrated in this paper is a first. Furthermore, the accelerometer can operate with a full-scale range between ±4g to ±16g and hence has enough dynamic range to measure tiny physiological vibrations as well as human gait and limb motion during strenuous physical activity.

RESULTS

To test out the functionality of the chest patch, it is placed on the chest of a healthy male and fixed using an elastic chest strap around the mitral valve (MV) region. The top plot in Figure 8 shows the time synchronized capture of both the SCG and ECG waveforms. This shows the raw data without any filtering. Alignment between the ECG and SCG allows for easy pickup of various peaks related to physiologic events that are part of the systolic and diastolic cycles. The labeled events include the mitral closure (MC), aortic opening (AO), rapid ejection (RE), mitral opening (MO), rapid filling (RF), atrial systole (AS), and aortic closure (AC).

To highlight the heart-sounds, the signals are high-pass filtered using a 45 Hz cut-off frequency. The bottom plot of Figure 8 shows the two main heart-sounds S_1 (closure of the atrioventricular valves) and S_2 (closure of the semilunar valves). The systole and diastole cycles can be easily identified. Of particular interest are the S_3 and S_4 heart sounds. The third heart sound (S_3) is a low-frequency, brief vibration occurring in early diastole at the end of rapid filling of the left or right ventricle. While children and adults <40 years of age may have a normal third heart sound, in later years it is usually

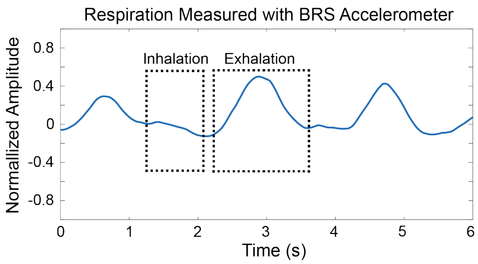

Figure 9. Respiration rate of intubated patient in the ER as measured using the BRS accelerometer.

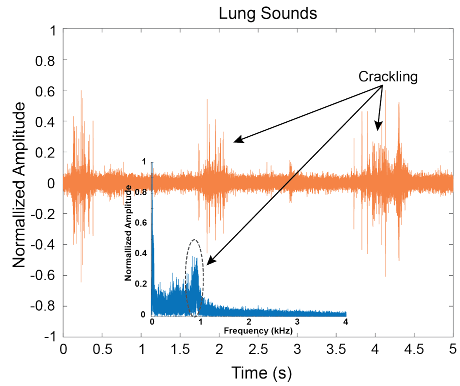

Figure 10. Lung-sounds recorded in the ER and revealing crackling due to pneumonia.

abnormal and may indicate dysfunction or volume overload of the ventricles [13]. S_3 is hard to see on the top plot in Figure 8 due to its low-frequency. It is mixed in with the RF peak. The fourth heart sound S_4 (not present in Figure 8) is coincident with late diastolic filling of the ventricle due to atrial contraction indicating resistance to the filling of either ventricle.

Normal lung function is difficult to identify even with a regular stethoscope. To assess lung-auscultation abnormal breathing is required. With requisite approval and test protocol in place, the chest patch is used to collect data on an emergency room patient. Because the patient is immobile and intubated, the chest patch was lightly placed on sternal manubrium without any further retaining method. Figure 9 shows the respiration rate as measured by the BRS accelerometer. A simple moving average filter with a 4000-pt window is used to smooth the curve. To identify the lung-sounds a high-pass filter with a cutoff of 500 Hz is used to produce the plot in Figure 10 (full-bandwidth data is used for the frequency response insert). The sound was identified to be a combination of wheezing and moist crackles (characteristic frequency response ~0.8-0.9 kHz). The SCG data compared to an electronic stethoscope recording underwent independent review by three cardiologists who all confirmed the diagnoses. With the technological framework in place, enhanced by the new BRS accelerometer capability, these results pave the way for wider clinical studies to better understand the capabilities. Further work is needed to reduce motion artifacts and improve the SNR.

CONCLUSION

This paper presented a multi-parameter vital-sign monitoring system for heart and lung auscultation. The chest patch is enabled through a new ultra-low-noise, wide-bandwidth, and low-power tri-axial accelerometer used for SCG and lung auscultation. The BRS accelerometer (ADXL380) has a noise density <30 µg/√Hz, a 4 kHz -3 dB bandwidth, and requires <400 µA, offering a new level of performance and power consumption that is enabling for wireless edge sensing applications such as this. Validation of the ability to collect SCG and lung sound data was demonstrated. The chest patch further integrates PPG and ECG capabilities for the simultaneous and synchronized collection of a multitude of vital-signs that can collectively be used to gain health insights about the patient.

ACKNOWLEDGEMENTS

The authors would like to thank the entire ADXL380 product development team at Analog Devices for their significant contribution to this work.

REFERENCES

[1] C. W. Tsao *et al.*, "Heart Disease and Stroke Statistics—2023 Update: A Report From the American Heart Association," *Circulation,* vol. 147, no. 8, pp. e93-e621, 2023.

[2] W. H. Organization. "Cardiovascular diseases." https://www.who.int/health-topics/cardiovascular-diseases (accessed April 5, 2024).

[3] D. E. Bloom *et al.*, "The global economic burden of noncommunicable diseases," Report in Program on the Global Demography of Aging, World Economic Forum, 2012.

[4] J. M. Zanetti and D. M. Salerno, "Seismocardiography: a technique for recording precordial acceleration," in *Proceedings of the Fourth Annual IEEE Symposium on Computer-Based Medical Systems,* 1991, pp. 4-9.

[5] Y. Kim *et al.*, "Respiratory sound classification for crackles, wheezes, and rhonchi in the clinical field using deep learning," *Scientific Reports,* vol. 11, no. 1, p. 17186, 2021.

[6] D. Vitazkova *et al.*, "Advances in Respiratory Monitoring: A Comprehensive Review of Wearable and Remote Technologies," *Biosensors (Basel),* vol. 14, no. 2, 2024.

[7] J.-Y. Yoo *et al.*, "Wireless broadband acousto-mechanical sensing system for continuous physiological monitoring," *Nature Medicine,* vol. 29, no. 12, pp. 3137-3148, 2023/12/01 2023.

[8] S. H. Lee *et al.*, "Fully portable continuous real-time auscultation with a soft wearable stethoscope designed for automated disease diagnosis," *Science Advances,* vol. 8, no. 21, p. eabo5867, 2022.

[9] P. Gupta, M. J. Moghimi, Y. Jeong, D. Gupta, O. T. Inan, and F. Ayazi, "Precision wearable accelerometer contact microphones for longitudinal monitoring of mechano-acoustic cardiopulmonary signals," *npj Digital Medicine,* vol. 3, no. 1, p. 19, 2020.

[10] F. Leitão *et al.*, "High-Resolution Seismocardiogram Acquisition and Analysis System," *Sensors (Basel),* vol. 18, no. 10, 2018.

[11] J. Lin *et al.*, "A 4 kHz, 25 µg/√Hz, 3-Axis MEMS Accelerometer ASIC Using Beyond-Resonant-Frequency Sensing," in *2023 IEEE Custom Integrated Circuits Conference (CICC)*, pp. 1-2, 2023

[12] S. Pavan, R. Schreier, and G. C. Temes, *Understanding Delta-Sigma Data Converters*. Wiley, 2017.

[13] H. K. Walker, W. D. Hall, and J. W. Hurst, *Clinical Methods: The History, Physical, and Laboratory Examinations*. Butterworths, 1990.

CONTACT

*Tzeno Galchev; tgalchev@gmail.com